Editors' Suggestion          Featured in Physics

# Direct observation of coherent magnons with suboptical wavelengths in a single-crystalline ferrimagnetic insulator

J. Förster [1,*] J. Gräfe [1] J. Bailey,[2,3] S. Finizio,[2] N. Träger,[1] F. Groß [1] S. Mayr,[2,4] H. Stoll,[1,5] C. Dubs [6] O. Surzhenko,[6]
N. Liebing,[7] G. Woltersdorf,[7] J. Raabe [2] M. Weigand,[1,8] G. Schütz,[1] and S. Wintz [1,2]

[1]*Max-Planck-Institut für Intelligente Systeme, 70569 Stuttgart, Germany*
[2]*Paul Scherrer Institut, 5232 Villigen PSI, Switzerland*
[3]*École Polytechnique Fédérale de Lausanne (EPFL), 1015 Lausanne, Switzerland*
[4]*Laboratory for Mesoscopic Systems, Department of Materials, ETH Zurich, 8092 Zurich, Switzerland*
[5]*Institut für Physik, Johannes Gutenberg-Universität Mainz, 55099 Mainz, Germany*
[6]*INNOVENT e.V. Technologieentwicklung Jena, 07745 Jena, Germany*
[7]*Institut für Physik, Martin Luther University Halle-Wittenberg, 06120 Halle, Germany*
[8]*Helmholtz-Zentrum Berlin, 14109 Berlin, Germany*

Spin-wave dynamics were studied in an extended thin film of single-crystalline yttrium iron garnet using time-resolved scanning transmission x-ray microscopy. A combination of mechanical grinding and focused ion beam milling has been utilized to achieve a soft x-ray transparent thickness of the underlying bulk gadolinium gallium garnet substrate. Damon-Eshbach type spin waves down to about 100 nm wavelength have been directly imaged in real space for varying frequencies and external magnetic fields. The dispersion relation extracted from the experimental data agreed well with theoretical predictions. A significant influence of the ion milling process on the local magnetic properties was not detected.

## I. INTRODUCTION

Spin waves are the fundamental excitations of ordered spin systems with the magnon being their quasiparticle of excitation. For almost 100 years, spin waves have been an active topic in magnetism research [1–4]. During this time, the ferrimagnetic insulator yttrium iron garnet (YIG) has stood out as platform for experimental studies on spin waves [3–6]. The reason for this lies in its exceptionally low intrinsic magnetic damping, which leads to very high spin-wave lifetimes and propagation lengths [7]. More recently, the idea of using spin waves as information carriers in novel computation logics [7–10] has triggered a rising interest in the subject referred to as magnonics. Combined with advances in optical spin wave measurement techniques like Brillouin light scattering (BLS) [7,8,11,12], and time-resolved Kerr effect microscopy (TR-MOKE) [13,14], as well as all-electrical spin-wave spectroscopy [6,15,16], this has lead to extensive studies of spin waves in various magnetic systems, in particular in thin magnetic films.

A relatively recent entry in spin-wave measurement techniques is time-resolved scanning transmission x-ray microscopy (TR-STXM). This technique provides direct imaging of dynamical magnetic phenomena with down to 10 nm spatial resolution. This is more than one order of magnitude higher than the resolution and wavelength sensitivity of state-of-the-art optical techniques (typically ≈250 nm). In addition, the contrast mechanism based on the XMCD effect [17] at the $L_2$ and $L_3$ absorption edges provides large magnetic contrast and offers element and even chemical sensitivity especially for $3d$ transition metals. The technique thus can offer insights into areas inaccessible to visible light optics. This in particular concerns spin waves of 250 nm wavelength or below, which are of great interest to the application oriented aspect of the field in terms of device miniaturization.

TR-STXM has been successfully demonstrated in imaging the dynamics of magnetic vortices and spin waves in metallic thin films [18–26]. However, applying this method to YIG proved to be challenging, as YIG needs to be grown on a single-crystalline substrate for achieving its ultimate dynamic properties [27]. Such a substrate is in general much too thick for sufficient soft x-ray transmission. Therefore, the substrate needs to be removed or thinned down substantially in order to overcome this obstacle, a demand that is shared with quantum-level magnon experiments at mK temperatures where paramagnetic resonances in the adjacent substrate may cause critical dissipation [28,29]. One possible way to achieve a soft x-ray transparent substrate level is cutting out a small, nearly substrate free lamella from the film using focused ion beam (FIB) milling. This approach has been successfully applied recently [30] but it restricts the lateral dimensions of the sample to a few microns and it also limits the means
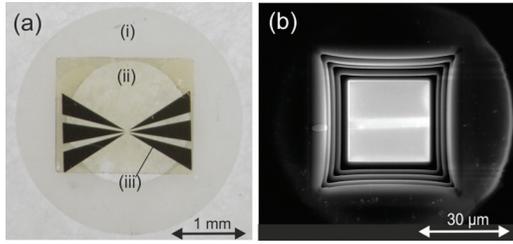
FIG. 1. (a) Optical micrograph of the 185 nm YIG film sample after substrate thinning. (i) Framing ceramic ring (aluminium oxide). (ii) YIG film on the remaining 20 $\mu$m thick GGG substrate. (iii) Copper stripline antennas (2 $\mu$m width in the center region). (b) SEM image of a FIB-milled x-ray window with stripline antenna visible on the other side.

for successive nanofabrication. An approach allowing for more general sample designs is utilizing a combination of mechanical grinding and FIB milling to create local areas of soft x-ray transparency in an extended bulk substrate [31,32]. By adopting this approach to TR-STXM, spin waves in an extended YIG thin film have been recorded with the main focus being on the excitation and imaging of spin waves with wavelengths below 250 nm.

For primary excitation a simple stripline antenna was utilized. Such an antenna is convenient to fabricate, but has a limited efficiency for the excitation of wavelengths smaller than its width. To alleviate this limitation, while avoiding very narrow antenna structures which are both difficult to fabricate and to impedance match, the edge demagnetization field of a disk of Permalloy ($Ni_{81}Fe_{19}$) was used in combination with interfacial exchange coupling as an effective antenna [33]. Exploiting this effective antenna in the TR-STXM, spin waves with wavelengths below the optical resolution limit of visible light, namely down to 100 nm wavelengths, have been observed in YIG.

## II. METHODS

Two YIG films of 185 nm and 80 nm respective thickness were grown by liquid phase epitaxy (LPE) on (111)-oriented gadolinium gallium garnet (GGG) of 0.5 mm thickness [27]. A saturation magnetization of $M = (143 \pm 2)$ kA/m was measured through vibrating sample magnetometry for a comparable 100 nm thick film fabricated at the same facility [27]. Gilbert damping coefficients of $\alpha = 0.3 \times 10^{-4}$ (185 nm) and $\alpha = 1.9 \times 10^{-4}$ (80 nm) have been determined via ferromagnetic resonance measurements. Both quantities agree well with typical values for YIG films in literature [7,27,34]. Stripline antennas of copper, each 2 $\mu$m wide and 80 nm thick [cf. Figs. 1(a) and 2], were deposited onto the 185 nm YIG film using e-beam lithography, sputtering, and subsequent lift-off processing. For the 80 nm YIG film a disk of Permalloy, 2 $\mu$m in diameter and 100 nm thick, was deposited first, with a copper antenna of 2 $\mu$m width and 200 nm thickness then deposited on top of it, both using e-beam lithography, thermal evaporation, and lift-off. The films were then cut into squares of 2 mm edge length with a wire saw such that each square contained a set of antennas near its center. For thinning down
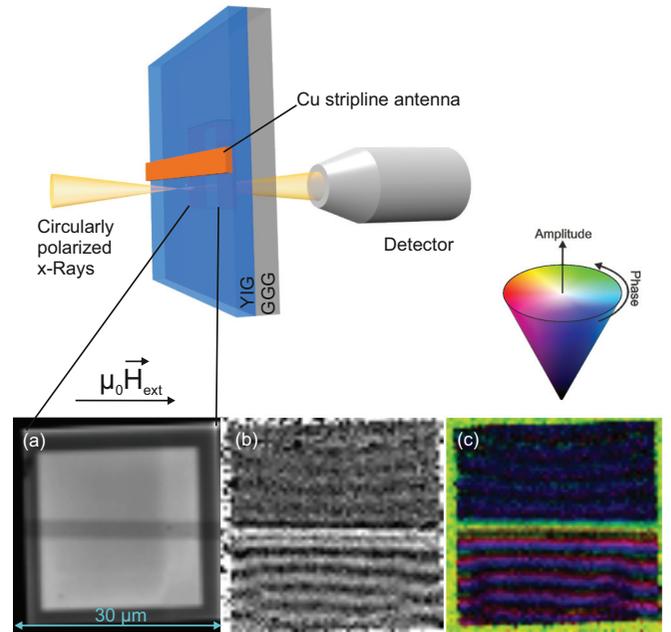


FIG. 2. Upper part: schematics of the sample architecture and measurement setup. Circularly polarized x rays are focused onto the sample region of the ion milled x-ray window in the GGG substrate. The x-ray transmission intensity is measured by a detector with an avalanche photodiode. Lower part: TR-STXM images of Damon-Eshbach geometry spin waves in the 185 nm thick YIG-film sample at an external magnetic bias field of $\mu_0 H_{ext} = 18$ mT and a frequency of $f = 2.5$ GHz. (a) Direct x-ray intensity image of the sample's transmission window. The central dark horizontal stripe is the antenna. (b) Single time frame of the time-resolved measurement with dynamical normalization that emphasizes the spin waves over the static background. Grayscale values represent the changes of the out-of-plane magnetization component. (c) Result of time-domain Fourier analysis, showing amplitude and phase of the waves in HSV (hue-saturation-value) color space (color code above the image).

the 0.5 mm thick GGG substrate, two different approaches were taken.

For the 185 nm YIG film the substrate was mechanically ground down uniformly to about 20 $\mu$m thickness using an *"Allied Techprep"* polishing device. A ring of aluminium oxide ceramic was glued onto the thinned sample for stability and as a handle (see Fig. 1). The substrate of the 80 nm YIG film was instead ground to about 90 $\mu$m thickness, leaving it stable enough to be handled without an additional ring. It was then further processed with a dimple grinder for thinning just an area around the center to the required 20 $\mu$m thickness. While the latter approach takes more time and restricts the accessible area on the sample, it offers a significant gain in stability. This results in the sample being easier to handle and less likely to break in subsequent processing steps. In the final step for both approaches rectangular x-ray transparent windows [cf. Fig. 1(b)] were carved into the remaining substrate by gallium ion milling using a focused ion beam microscope (FEI *NovaNanoLab* 600 *DualBeam*). The window area was $30 \times 30$ $\mu$m$^2$ for the 185 nm sample and $50 \times 80$ $\mu$m$^2$ for the 80 nm sample, respectively. The thickness of the remaining substrate therein was estimated using electron transparency to

be approximately between 60 nm and 200 nm for the 185 nm YIG film, and between 140 nm and 300 nm for the 80 nm YIG film, respectively.

Measurements have been carried out at the MAXYMUS end station of the BESSY II synchrotron radiation facility of Helmholtz-Zentrum Berlin. Circularly polarized x rays were focused to a spot of 18 nm diameter using a diffractive Fresnel zone plate. The x-ray energy was always set to one of the three local maxima of the dichroic signal at the iron $L_3$-absorption edge ($E \sim 710$ eV) [35]. Time-resolved measurements were achieved by using a stroboscopic pump-and-probe technique, for which the temporal resolution is given by the time spread of the probing x-ray flashes, i.e., $\sim 70$ ps during the synchrotron's regular multibunch mode operation and $\sim 10$ ps in the low alpha mode [24] (contributions from the electronic pump signal of the experiment are usually negligible in comparison).

The samples were mounted either in normal (90°) or 60° x-ray incidence geometry for different measurements. The first configuration provided pure sensitivity to the out-of-plane component of the magnetization, while the latter gave a mixed signal of out-of-plane and in-plane components. A magnetic bias field in the sample plane was set via a quadrupole permanent magnet system [36]. Alternating currents between 5 and 17 mA amplitude running through the copper striplines on the YIG films' surfaces excited the magnetization dynamics in the samples by generating time-dependent magnetic fields of approximately 1.5 to 5 mT magnitude (in-plane) [37]. After recording, the raw movies from TR-STXM were normalized and a subsequent fast Fourier transform (FFT) in time was used to obtain both the local spin-wave amplitude and phase [38,39]. Via a two-dimensional spatial FFT the corresponding wave vectors were determined.

## III. EXPERIMENTAL RESULTS

Figure 2 displays an example of a recorded spin wave in a 185 nm YIG-film sample. For this thicker sample the x-ray energy was set to the first of the three XMCD maxima in order to maximize transmission [35]. Part (a) shows the direct x-ray image of the ion beam etched window, with one stripline antenna being clearly visible as a darker bar in the center. Slight inhomogeneities in the window thickness, indicated by the intensity differences, can be noted, especially on the right edge. Image (b) features a frame of the corresponding dynamic movie recorded for an excitation frequency of $f =$ 2.5 GHz and an external magnetic field of $\mu_0 H_{\text{ext}} = 18$ mT. The raw data was normalized by dividing each point of the frames by its time average. This procedure suppresses the static background and thus emphasizes the time-dependent magnetic contrast. As expected in the Damon-Eshbach (DE) configuration, the waves propagate perpendicular to the magnetic field from the stripline towards the window edges. A strong asymmetry in amplitude can be observed between waves propagating to the upper and lower edge. This well-known emission characteristic of DE-geometry waves can be attributed to the asymmetry of the antenna's out-of-plane excitation field component [40]. Fourier phase and amplitude of the wave are shown in image (c). The wave fronts appear to be mostly straight and only mildly perturbed by the window
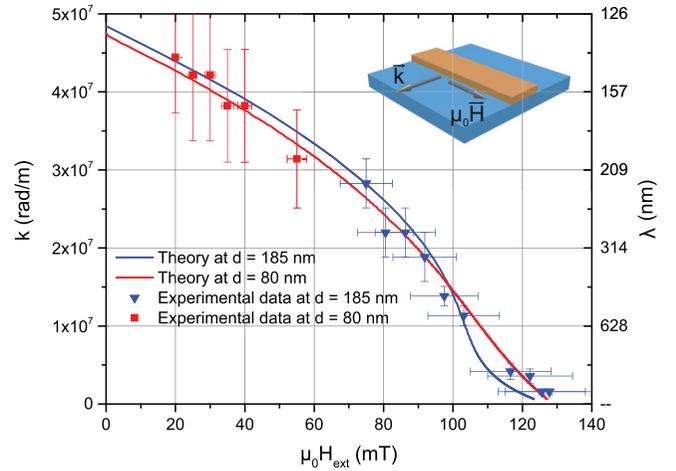


FIG. 3. Measured wave vectors and wavelengths of stripline excited spin waves in Damon-Eshbach configuration (see schematic in the upper right corner) at varying magnetic bias fields at a constant frequency $f = 5.5$ GHz in YIG films of thickness $d = 185$ nm (blue triangles) and $d = 80$ nm (red squares). The lines of corresponding color represent the theoretically predicted values according to Eq. (1).

edges rather than by the inhomogeneous window thickness. This indicates that the ion beam did not induce noticeable morphological or magnetic inhomogeneities in the YIG itself. The small wave perturbations close to the frame are presumably either a result of a slight temperature gradient between the YIG regions with substantially different GGG substrate thicknesses, for which the ohmic losses primarily in the narrow part of the stripline are the primary heat source, or a consequence of a potential stress difference in the YIG film for regions of different GGG substrate thickness.

In order to map the corresponding spin-wave dispersion characteristics and to find the shortest wavelengths excitable by the stripline antenna in the given samples, the external magnetic field was varied from 130 down to 20 mT over a measurement series at a constant frequency of $f = 5.5$ GHz. The measured wavelengths ($\lambda$), respectively their inverse wave numbers ($k = 2\pi/\lambda$), were then compared to the dispersion of DE geometry waves predicted by theory [41]. When intermodal hybridization is neglected, following Ref. [41], the dispersion equation for the fundamental mode in question (uniform thickness distribution of amplitude and phase) is given by

$$f = \frac{\gamma \mu_0}{2\pi} \left\{ \left( H + \frac{2A}{\mu_0 M} k^2 \right) \left( H + \frac{2A}{\mu_0 M} k^2 + M F_{00} \right) \right\}^{1/2}, \quad (1)$$

with $\gamma = 1.76 \times 10^{11}$ rad/(s T) being the gyromagnetic ratio, $\mu_0 = 4\pi \times 10^{-7}$ V s/(A m) the vacuum permeability, $A = 0.36 \times 10^{-11}$ J/m (cf. Ref. [42]) the exchange constant, $d$ the film thickness, $M$ the saturation magnetization (see above), and $F_{00}$ the element of the dipole-dipole matrix:

$$F_{00} = 1 + \frac{1 - e^{-kd}}{kd} \left( 1 - \frac{1 - e^{-kd}}{kd} \right) \frac{M}{H + \frac{2A}{\mu_0 M} k^2}. \quad (2)$$

Figure 3 displays the experimental results of the field variation series at the constant frequency of $f = 5.5$ GHz for the

two film thicknesses. X-ray energy for the thinner 80 nm thick sample was set to the central (largest) of the XMCD peaks. Blue triangles represent measurements at $d = 185$ nm, while the red squares stand for those at $d = 80$ nm, respectively. The lines of corresponding color show theoretically predicted values according to Eq. (1), with which the experimental data reasonably agrees. It should be noted that the neglect of hybridization effects leading to Eq. (1) is not necessarily a valid approximation for the 185 nm film in case of short wavelengths. It has been shown in an earlier experiment [30] that in a YIG film of this thickness hybridization between the fundamental and the first higher order mode in DE geometry can significantly affect the dispersion relation [24,41]. This apparently not being the case here can be explained by the comparatively much higher external magnetic fields applied, which lead to the higher order mode shifting upwards in frequency and no longer crossing the fundamental mode. Spin waves have been recorded down to 220 nm wavelength at 185 nm film thickness and down to 140 nm in the 80 nm thick film. In both cases there was no more spin wave activity detectable at lower fields despite that the amplitude of the excitation current was close to the expected damage threshold of the stripline antennas. As the spin-wave excitation efficiency of a stripline decreases rapidly (in an oscillatory way) for wavelengths below the antenna width of 2 $\mu$m [43], we concluded that a possible excitation of shorter waves than the ones detected would have required driving currents potentially dangerous to the sample and we thus did not pursue this route further.

It is notable that the excitation limit towards smaller wavelengths is considerably lower in the 80 nm thick film than in the 185 nm one. A possible explanation for this lies in the broadening of the antenna's Oersted field distribution in the YIG film with increasing distance from the stripline. This results in an overall higher effective width of the antenna in thicker films. While the antenna's thickness also plays a role in this regard, its influence is small in comparison (cf. Fig. S1 in the Supplemental Material [44]). The results above clearly demonstrate that it is possible to use a stripline antenna for the excitation of spin waves with wavelengths below the optical resolution limit of visible light in the 80 nm YIG film. However, this is realized at high input powers resulting in only relatively low spin-wave amplitudes. This situation can be improved by exploiting the Permalloy disk patterned onto the 80 nm YIG film (cf. Fig. 4, upper part).

It has been shown that local magnetic formations such as domain walls [45–47], edge bound demagnetizing fields [33,48,49], or vortices [23,24,50] can function as spin wave emitters offering effective "antenna" widths well below 200 nm. A major advantage of this approach is that the devices providing such formations are a lot larger than these effective widths. Thus, compared to an actual antenna of such small size, they are a lot easier to fabricate and to impedance match. At the same time, they are also less delicate, i.e., able to carry more input power.

The Permalloy disk contained a magnetic vortex structure that imprints to the YIG film below through magnetic interlayer coupling. Inset (a) in Fig. 4 shows a micromagnetic simulation [51] (using *"MuMax 3"* [52]) of the YIG film's in-plane ground state below the disk at $\mu_0 H_{ext} = 5$ mT, which
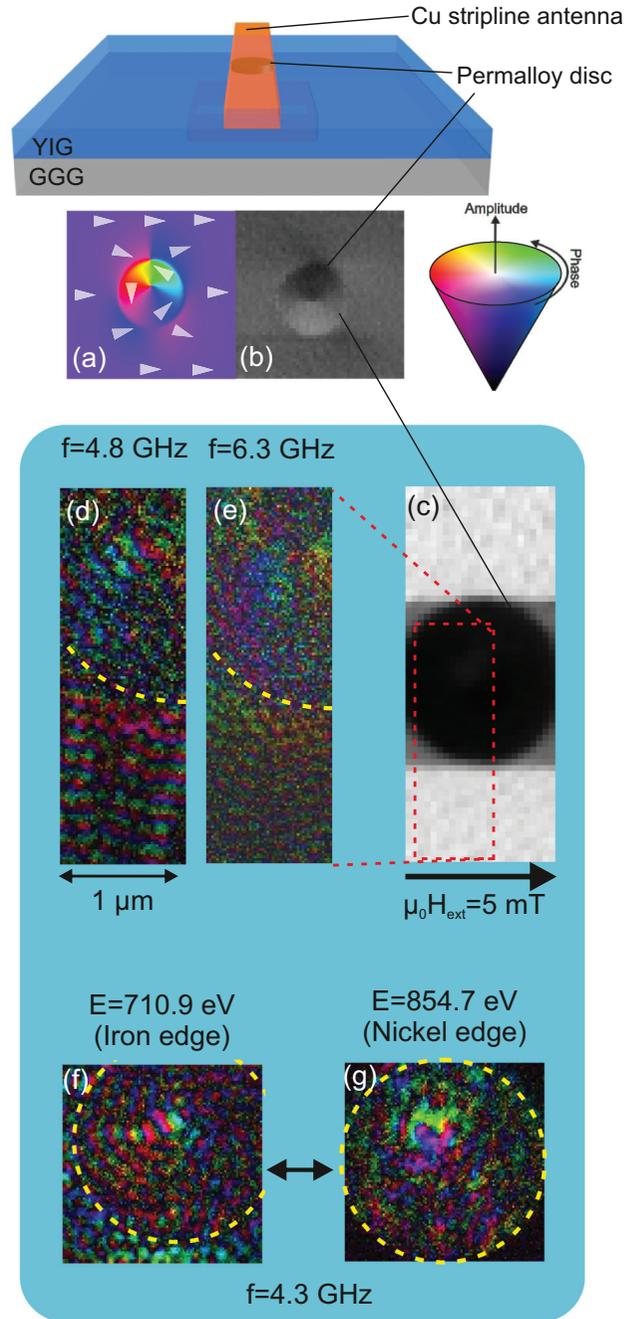


FIG. 4. Upper part: schematics of the 80 nm YIG film sample with the 2 $\mu$m diameter Permalloy disk beneath the antenna. (a) Micromagnetic simulation of the in-plane magnetization in YIG below a Permalloy disk. (b) Corresponding STXM measurement of the in-plane magnetization in the sample at the iron $L_3$ edge. Grayscale intensity indicates the horizontal in-plane magnetization component. (c) X-ray transmission image of the region around the disk (black area). The antenna is visible as dark gray areas surrounding the disk. (d),(e) Examples of spin wave measurements in the sector indicated by the red dotted rectangle in (c) displayed in HSV color-space representation [color code next to (b)]. The yellow dotted line marks the disk's edge. Measurements were taken at $f = 4.8$ GHz and $f = 6.3$ GHz, respectively, at a field of $\mu_0 H_{ext} = 5$ mT. (f),(g) HSV-color images of measurements in the Permalloy disk covered area at $\mu_0 H_{ext} = 5$ mT and $f = 4.3$ GHz at two different x-ray energies (iron edge for YIG + Permalloy; nickel edge for Permalloy only).

supports this assumption. Inset (b) shows a static STXM measurement of the disk at the iron $L_3$ edge (at the lowest energy XMCD peak) at the same field and 60° incidence angle. The gray scale contrast represents a combination of the horizontal in-plane magnetization component (white means it is pointing to the right) and the out-of-plane component (which is close to zero here except for the core). A typical vortex pattern can be observed with the in-plane magnetization oriented to the right in the lower disk quadrant and opposite in the upper quadrant with an intermediate state in the side quadrants. Since the measurement combines magnetic contrast of YIG and Permalloy it is unfortunately not a definite proof that the vortex actually extends to the YIG film. However, the later appearance of radial spin waves in the region covered by the disk in our dynamic measurements strongly points to that being the case.

The disk thus provided potential wave emitting structures through the vortex core as well as by the inhomogenous dynamic demagnetizing fields at the edge of the disk, both excitable by the field of the stripline antenna covering it (cf. Fig. 4, upper part). Note that in this configuration there is also an antivortex forming in the YIG film at the upper disk boundary for continuity reasons [cf. Fig. 4(a), upper disk edge]. This did, however, not notably affect the resulting wave emission pattern and is thus disregarded in the following. Image (c) in Fig. 4 shows an x-ray transmission image of the disk (black circle) and the surrounding area. Next to it in (d) and (e) are two exemplary spin wave measurements at two different frequencies made in the area indicated by the red dotted rectangle in (c). The pictures show Fourier amplitude and phase in the HSV color representation given by the color code next to (b). Spin waves propagate away from the lower edge of the disk area in DE geometry (boundary marked by the yellow dotted line). The wavelength of these is visibly shorter in image (e) ($f = 6.3$ GHz) compared to (d) ($f = 4.8$ GHz) as expected for DE-geometry waves. Additionally, inside the disk area in (d) radial waves propagate from a point in the disk center to the edge. This can be observed more clearly in image (f) at $f = 4.3$ GHz, where a wider section of the disk has been imaged. This behavior strongly hints at a vortex structure with the core as a wave source (cf. Refs. [23,24,50]). As this measurement, again, combines signals from the YIG and the Permalloy, to make sure that the radial waves and the implied vortex are indeed in the YIG film, a second measurement at the same frequency was conducted at the $L_3$ edge of nickel. The result is presented in image (g) in Fig. 4. This measurement solely contains the spin dynamics in the Permalloy disk which is clearly different from the radial waves shown in images (f) and (d). It can be concluded that these waves, as well as a vortex structure, are indeed located in the YIG film.

Since the radial waves in the disk area appear to vanish beyond $f = 6$ GHz while the waves emitted from the lower edge still continue [cf. Fig. 4(e)], it can be concluded that those are independent from each other. Since the edge emission continues to comparatively higher frequencies and lower wavelengths, the focus of the remaining work will be solely on these while the vortex core driven dynamic will be disregarded. The dispersion relation of the edge emitted
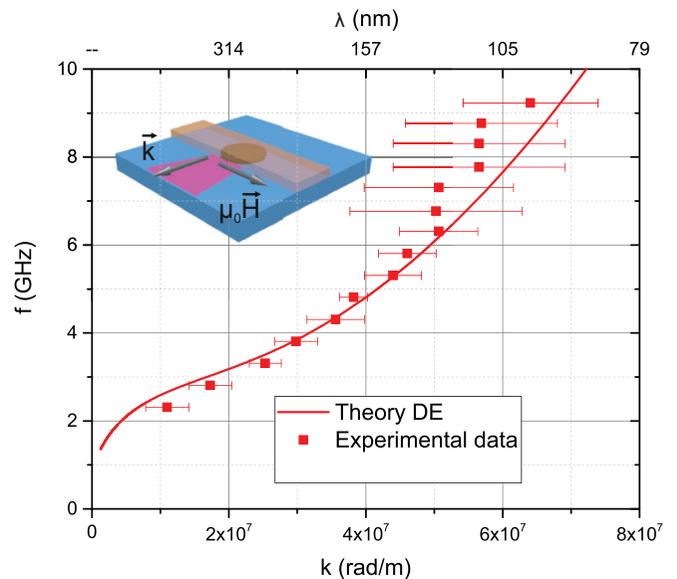


FIG. 5. Measured dispersion relation (squares) of spin waves in the YIG film emitted from the bottom edge of the disk at $\mu_0 H_{ext} = 5$ mT. The line graph depicts the theoretical predictions according to Eq. (1). The schematic on the upper left depicts the measurement geometry and area (purple) on the sample.

waves measured at $\mu_0 H_{ext} = 5$ mT is displayed in Fig. 5. On the upper left a schematic of the sample indicates the area in which the data has been acquired in purple. The red line represents the theoretical dispersion based on Eq. (1) in the frequency interval from $f = 1.5$ GHz to $f = 10$ GHz, which has been covered in the experiment. For most of this interval the dispersion is in the dipole-exchange regime where the exchange terms, that are quadratic in $k$, become increasingly influential with increasing frequencies. Experimental data fit the theoretical values reasonably up to $f \approx 7$ GHz. Some light inaccuracies are to be expected due to the low external field strength, which emphasizes intrinsic out-of-plane field offsets of the quadrupole permanent magnet. Beyond 7 GHz the uncertainty of the $k$ vectors increases due to the decrease of the selected measurement area. This has been done to keep measurement durations at a reasonable level while necessarily increasing spatial resolution and integration time to still detect the dynamic signal. Regardless of this the theoretical curve lies within the uncertainty margin of the measured $k$ vectors. Measurements were continued towards higher frequencies until no spin waves could be detected at maximum input power anymore. The lowest observed wavelength was about 100 nm, unambiguously beyond the optical resolution range and also beyond what has been achieved with the stripline antenna. Additionally the microwave input power required for noticeable excitation was a factor of 5 lower compared to the bare stripline antenna at the same wavelength.

## IV. CONCLUSIONS

This work demonstrates the application of time-resolved STXM for the imaging of spin dynamics in extended single-crystalline YIG thin films. This was achieved through a

combination of mechanical grinding and FIB milling in order to reduce the substrate thickness to a sufficiently x-ray transparent level. Spin wave dynamics have been recorded in the Damon-Eshbach geometry for various frequencies and external magnetic fields. Wavelengths were determined and compared to theoretical predictions, which they reasonably agreed with. There was no noticeable impact of the thinning process detected with respect to the spin-wave dispersion relation or the spatial wave distribution. By using stripline antennas, spin waves were observed at wavelengths below the visible light resolution limit at moderate excitation efficiencies. Yet, utilizing the dynamic demagnetizing field on the edge of a Permalloy disk as emitter together with interfacial exchange coupling, spin waves of down to 100 nm wavelengths were efficiently excited and directly imaged. These results provide further insight into the nanoscale spin-wave dynamics in low damping magnonic systems both in terms of fundamental aspects and applications.

[1] F. Bloch, Zur theorie des ferromagnetismus, Z. Phys. **61**, 206 (1930).

[2] R. W. Damon and J. R. Eshbach, Magnetostatic modes of a ferromagnet slab, J. Phys. Chem. Solids **19**, 308 (1961).

[3] J. R. Eshbach, Spin-Wave Propagation and the Magnetoelastic Interaction in Yttrium Iron Garnet, Phys. Rev. Lett. **8**, 357 (1962).

[4] R. W. Damon and H. van de Vaart, Dispersion of spin waves and magnetoelastic waves in YIG, Proc. IEEE **53**, 348 (1965).

[5] W. Schilz, Experimental evidence for coupling between dipole and exchange dominated spin waves in epitaxial YIG, Solid State Commun. **11**, 615 (1972).

[6] M. Kaack, S. Jun, S. A. Nikitov, and J. Pelzl, Magnetostatic spin wave modes excitation in yttrium iron garnet film under various temperatures, J. Magn. Magn. Mater. **204**, 90 (1999).

[7] A. A. Serga, A. V. Chumak, and B. Hillebrands, YIG magnonics, J. Phys. D: Appl. Phys. **43**, 264002 (2010).

[8] A. V. Chumak, V. I. Vasyuchka, A. A. Serga, and B. Hillebrands, Magnon spintronics, Nat. Phys. **11**, 453 (2015).

[9] V. V. Kruglyak, S. O. Demokritov, and D. Grundler, Magnonics, J. Phys. D: Appl. Phys. **43**, 264001 (2010).

[10] T. Fischer, M. Kewenig, D. A. Bozhko, A. A. Serga, I. I. Syvorotka, F. Ciubotaru, C. Adelmann, B. Hillebrands, and A. V. Chumak, Experimental prototype of a spin-wave majority gate, Appl. Phys. Lett. **110**, 152401 (2017).

[11] T. Sebastian, K. Schultheiss, B. Obry, B. Hillebrands, and H. Schultheiss, Micro-focused Brillouin light scattering: imaging spin waves at the nanoscale, Front. Phys. **3**, 35 (2015).

[12] M. Collet, O. Gladii, M. Evelt, V. Bessonov, L. Soumah, P. Bortolotti, S. O. Demokritov, Y. Henry, V. Cros, M. Bailleul, V. E. Demidov, and A. Anane, Spin-wave propagation in ultra-thin YIG based waveguides, Appl. Phys. Lett. **110**, 092408 (2017).

[13] A. Talalaevskij, M. Decker, J. Stigloher, A. Mitra, H. S. Körner, O. Cespedes, C. H. Back, and B. J. Hickey, Magnetic properties of spin waves in thin yttrium iron garnet films, Phys. Rev. B **95**, 064409 (2017).

[14] J. P. Park, P. Eames, D. M. Engebretson, J. Berezovsky, and P. A. Crowell, Spatially Resolved Dynamics of Localized Spin-Wave Modes in Ferromagnetic Wires, Phys. Rev. Lett. **89**, 277201 (2002).

[15] H. Yu, O. d' Allivy Kelly, V. Cros, R. Bernard, P. Bortolotti, A. Anane, F. Brandl, F. Heimbach, and D. Grundler, Approaching soft x-ray wavelengths in nanomagnet-based microwave technology, Nat. Commun. **7**, 11255 (2016).

[16] M. Bailleul, D. Olligs, and C. Fermon, Propagating spin wave spectroscopy in a permalloy film: A quantitative analysis, Appl. Phys. Lett. **83**, 972 (2003).

[17] G. Schütz, W. Wagner, W. Wilhelm, P. Kienle, R. Zeller, R. Frahm, and G. Materlik, Absorption of Circularly Polarized X Rays in Iron, Phys. Rev. Lett. **58**, 737 (1987).

[18] H. Stoll, A. Puzic, B. van Waeyenberge, P. Fischer, J. Raabe, M. Buess, T. Haug, R. Höllinger, C. Back, D. Weiss, and G. Denbeaux, High-resolution imaging of fast magnetization dynamics in magnetic nanostructures, Appl. Phys. Lett. **84**, 3328 (2004).

[19] B. Van Waeyenberge, A. Puzic, H. Stoll, K. W. Chou, T. Tyliszczak, R. Hertel, M. Fähnle, H. Brückl, K. Rott, G. Reiss, I. Neudecker, D. Weiss, C. H. Back, and G. Schütz, Magnetic vortex core reversal by excitation with short bursts of an alternating field, Nature (London) **444**, 461 (2006).

[20] M. Noske, A. Gangwar, H. Stoll, M. Kammerer, M. Sproll, G. Dieterle, M. Weigand, M. Fähnle, G. Woltersdorf, C. H. Back, and G. Schütz, Unidirectional sub-100-ps magnetic vortex core reversal, Phys. Rev. B **90**, 104415 (2014).

[21] S. Bonetti, R. Kukreja, Z. Chen, F. Macià, J. M. Hernàndez, A. Eklund, D. Backes, J. Frisch, J. Katine, G. Malm, S. Urazhdin, A. D. Kent, J. Stöhr, H. Ohldag, and H. A. Dürr, Direct observation and imaging of a spin-wave soliton with p-like symmetry, Nat. Commun. **6**, 8889 (2015).

[22] J. Gräfe, M. Decker, K. Keskinbora, M. Noske, P. Gawronski, H. Stoll, C. H. Back, E. J. Goering, and G. Schütz, X-ray microscopy of spin wave focusing using a Fresnel zone plate, arXiv:1707.03664 [cond-mat.mes-hall].

[23] S. Wintz, V. Tiberkevich, M. Weigand, J. Raabe, J. Lindner, A. Erbe, A. Slavin, and J. Fassbender, Magnetic vortex cores as tunable spin-wave emitters, Nat. Nanotechnol. **11**, 948 (2016).

[24] G. Dieterle, J. Förster, H. Stoll, A. S. Semisalova, S. Finizio, A. Gangwar, M. Weigand, M. Noske, M. Fähnle, I. Bykova, J. Gräfe, D. A. Bozhko, H. Yu. Musiienko-Shmarova, V. Tiberkevich, A. N. Slavin, C. H. Back, J. Raabe, G. Schütz, and

S. Wintz, Coherent Excitation of Heterosymmetric Spin Waves with Ultrashort Wavelengths, Phys. Rev. Lett. **122**, 117202 (2019).

[25] M. Kammerer, M. Weigand, M. Curcic, M. Noske, M. Sproll, A. Vansteenkiste, B. Van Waeyenberge, H. Stoll, G. Woltersdorf, C. H. Back, and G. Schuetz, Magnetic vortex core reversal by excitation of spin waves, Nat. Commun. **2**, 279 (2011).

[26] S. Finizio, S. Wintz, K. Zeissler, A. V. Sadovnikov, S. Mayr, S. A. Nikitov, C. H. Marrows, and J. Raabe, Dynamic imaging of the delay- and tilt-free motion of neel domain walls in perpendicularly magnetized superlattices, Nano Lett. **19**, 375 (2019).

[27] C. Dubs, O. Surzhenko, R. Linke, A. Danilewsky, U. Brückner, and J. Dellith, Sub-micrometer yttrium iron garnet LPE films with low ferromagnetic resonance losses, J. Phys. D: Appl. Phys. **50**, 204005 (2017).

[28] S. Kosen, A. F. van Loo, D. A. Bozhko, L. Mihalceanu, and A. D. Karenowska, Microwave magnon damping in YIG films at millikelvin temperatures, APL Mater. **7**, 101120 (2019).

[29] L. Mihalceanu, V. I. Vasyuchka, D. A. Bozhko, T. Langner, A. Yu. Nechiporuk, V. F. Romanyuk, B. Hillebrands, and A. A. Serga, Temperature-dependent relaxation of dipole-exchange magnons in yttrium iron garnet films, Phys. Rev. B **97**, 214405 (2018).

[30] J. Förster, S. Wintz, J. Bailey, S. Finizio, E. Josten, C. Dubs, D. A. Bozhko, H. Stoll, G. Dieterle, N. Träger, J. Raabe, A. N. Slavin, M. Weigand, J. Gräfe, and G. Schütz, Nanoscale x-ray imaging of spin dynamics in yttrium iron garnet, J. Appl. Phys. **126**, 173909 (2019).

[31] J. Simmendinger, S. Ruoss, C. Stahl, M. Weigand, J. Gräfe, G. Schütz, and J. Albrecht, Transmission x-ray microscopy at low temperatures: Irregular supercurrent flow at small length scales, Phys. Rev. B **97**, 134515 (2018).

[32] M. Fohler, S. Frömmel, M. Schneider, B. Pfau, C. M. Günther, M. Hennecke, E. Guehrs, L. Shemilt, D. Mishra, D. Berger, S. Selve, D. Mitin, M. Albrecht, and S. Eisebitt, A general approach to obtain soft x-ray transparency for thin films grown on bulk substrates, Rev. Sci. Instrum. **88**, 103701 (2017).

[33] C. S. Davies, A. V. Sadovnikov, S. V. Grishin, Yu P. Sharaevskii, S. A. Nikitov, and V. V. Kruglyak, Generation of propagating spin waves from regions of increased dynamic demagnetising field near magnetic antidots, Appl. Phys. Lett. **107**, 162401 (2015).

[34] A. Krysztofik, L. E. Coy, P. Kuświk, K. Załski, H. Głowiński, and J. Dubowik, Ultra-low damping in lift-off structured yttrium iron garnet thin films, Appl. Phys. Lett. **111**, 192404 (2017).

[35] H. B. Vasili, B. Casals, R. Cichelero, F. Macià, J. Geshev, P. Gargiani, M. Valvidares, J. Herrero-Martin, E. Pellegrin, J. Fontcuberta, and G. Herranz, Direct observation of multivalent states and $4f \rightarrow 3d$ charge transfer in Ce-doped yttrium iron garnet thin films, Phys. Rev. B **96**, 014433 (2017).

[36] D. Nolle, M. Weigand, P. Audehm, E. Goering, U. Wiesemann, C. Wolter, E. Nolle, and G. Schütz, Note: Unique characterization possibilities in the ultra high vacuum scanning transmission x-ray microscope (UHV-STXM) maxymus using a rotatable permanent magnetic field up to 0.22 T, Rev. Sci. Instrum. **83**, 046112 (2012).

[37] F. Groß, N. Träger, J. Förster, M. Weigand, G. Schütz, and J. Gräfe, Nanoscale detection of spin wave deflection angles in permalloy, Appl. Phys. Lett. **114**, 012406 (2019).

[38] T. E. Oliphant, Python for scientific computing, Comput. Sci. Eng. **9**, 10 (2007).

[39] J. D. Hunter, Matplotlib: A 2D graphics environment, Comput. Sci. Eng. **9**, 90 (2007).

[40] T. Schneider, A. A. Serga, T. Neumann, B. Hillebrands, and M. P. Kostylev, Phase reciprocity of spin-wave excitation by a microstrip antenna, Phys. Rev. B **77**, 214411 (2008).

[41] B. A. Kalinikos and A. N. Slavin, Theory of dipole-exchange spin wave spectrum for ferromagnetic films with mixed exchange boundary conditions, J. Phys. C: Solid State Phys. **19**, 7013 (1986).

[42] S. Klingler, A. V. Chumak, T. Mewes, B. Khodadadi, C. Mewes, C. Dubs, O. Surzhenko, B. Hillebrands, and A. Conca, Measurements of the exchange stiffness of YIG films using broadband ferromagnetic resonance techniques, J. Phys. D: Appl. Phys. **48**, 015001 (2015).

[43] V. Sluka, T. Schneider, R. A. Gallardo, A. Kákay, M. Weigand, T. Warnatz, R. Mattheis, A. Roldán-Molina, P. Landeros, V. Tiberkevich, A. N. Slavin, G. Schütz, A. Erbe, A. Deac, J. Lindner, J. Raabe, J. Fassbender, and S. Wintz, Emission and propagation of 1d and 2d spin waves with nanoscale wavelengths in anisotropic spin textures, Nat. Nanotechnol. **14**, 328 (2019).

[44] See Supplemental Material at http://link.aps.org/supplemental/10.1103/PhysRevB.100.214416 for calculations of the antenna efficiency for the two antenna profiles and film thicknesses.

[45] S. J. Hermsdoerfer, H. Schultheiss, C. Rausch, S. Schäfer, B. Leven, S.-K. Kim, and B. Hillebrands, A spin-wave frequency doubler by domain wall oscillation, Appl. Phys. Lett. **94**, 223510 (2009).

[46] N. J. Whitehead, S. A. R. Horsley, T. G. Philbin, A. N. Kuchko, and V. V. Kruglyak, Theory of linear spin wave emission from a bloch domain wall, Phys. Rev. B **96**, 064415 (2017).

[47] R. B. Holländer, C. Müller, J. Schmalz, M. Gerken, and J. McCord, Magnetic domain walls as broadband spin wave and elastic magnetization wave emitters, Sci. Rep. **8**, 13871 (2018).

[48] B. Van de Wiele, S. J. Hämäläinen, P. Baláž, F. Montoncello, and S. van Dijken, Tunable short-wavelength spin wave excitation from pinned magnetic domain walls, Sci. Rep. **6**, 21330 (2016).

[49] F. B. Mushenok, R. Dost, C. S. Davies, D. A. Allwood, B. J. Inkson, G. Hrkac, and V. V. Kruglyak, Broadband conversion of microwaves into propagating spin waves in patterned magnetic structures, Appl. Phys. Lett. **111**, 042404 (2017).

[50] C. Behncke, C. F. Adolff, N. Lenzing, M. Hänze, B. Schulte, M. Weigand, G. Schütz, and G. Meier, Spin-wave interference in magnetic vortex stacks, Commun. Phys. **1**, 50 (2018).

[51] Simulation parameters for *"MuMax 3"*: YIG film: $M = 140$ kA/m, $A = 0.36 \times 10^{-11}$ J/m, $\alpha = 0.0001$; initial magnetization: uniform(0,1,0); Permalloy disk: $M = 760$ kA/m, $A = 1.30 \times 10^{-11}$ J/m, $\alpha = 0.05$; initial magnetization: Vortex(1,1); $B_{\text{ext}} = 5$ mT (y direction); world size: $5 \times 5 \times 0.18 \, \mu m^3$; mesh size: $512 \times 512 \times 16$ points .

[52] A. Vansteenkiste, J. Leliaert, M. Dvornik, M. Helsen, F. Garcia-Sanchez, and B. Van Waeyenberge, The design and verification of MuMax3, AIP Adv. **4**, 107133 (2014).